



Contents lists available at ScienceDirect

Optik

journal homepage: www.elsevier.com/locate/ijleo

Study of the optical properties of ZnO semiconductor nanoparticles using *Origanum vulgare* and its effect in Rhodamine B degradation

P.A. Luque^{a,*}, H.E. Garrafa-Gálvez^a, C.A. García-Maró^b, C.A. Soto-Robles^{c,**}

^a Universidad Autónoma de Baja California, Facultad de Ingeniería, Arquitectura y Diseño, C.P. 22860 Ensenada, BC, México

^b Departamento de Investigación en Polímeros y Materiales, Universidad de Sonora, Hermosillo 83000, Sonora, México

^c Tecnológico Nacional de México/IT de Los Mochis, C.P.81259 Los Mochis, Sinaloa, México

ARTICLE INFO

Keywords:

Rhodamine B
Nanoparticle biosynthesis
Photocatalysis
Origanum vulgare
ZnO

ABSTRACT

In this work, the effects of different *Origanum vulgare* extract concentrations on the green synthesis of zinc oxide nanoparticles (ZnO NPs) were studied and their effects on the Band gap values and photocatalytic application in Rhodamine B (RhB) degradation. During the green synthesis of ZnO NPs, a zinc ion source is used as the metal precursor and another of natural extracts as stabilizing agents; with this regard, here in *Origanum vulgare* extracts were used at 0.1%, 0.5% and 4% (% weight-volume). In order to define the ZnO NPs properties, they were characterized by FTIR, XRD, UV-Vis, HR-TEM, XPS and photoluminescence. In the FTIR analysis, the Zn-O bond can be seen at 384 cm^{-1} ; by means of XRD, the hexagonal crystalline phase of ZnO is distinguished (Wurtzite). The extract concentration used influences the ZnO NPs crystallite size and Band gap values as well as the degradation percentage of RhB. The ZnO NPs hold irregular shapes, the majority of which are oval with certain spherical tendencies and they vary in size distribution, which ranges from 37 to 8 nm, the smallest sizes resulting from the highest extract concentrations. The Band gap values are 2.94, 2.77, and 2.29 eV for ZnO-OV-0.1%, ZnO-OV-0.5% and ZnO-OV-4%, respectively, rising as the extract concentrations increase. These materials present good photocatalytic activity, nonetheless, the ZnO NPs synthesized using 4% extract showed the best results, degrading 94.24% of RhB in 100 min in UV light and 93% in 180 min in solar light.

1. Introduction

As progress evolves along the years, the dyes used in various industries, such as textile and food, have become an important source of pollutants for the environment, mainly for water. Alongside, the scientific community has worked on improving and being selective with their water treatment methods pertaining to certain contaminants [1]. There exist several water treatment techniques for this type of contaminants; although, photocatalysis represents an advanced technology that eliminates dyes. This technique is considered feasible, fast and effective for organic pollutants, decreasing the generation of secondary contaminants [2]. Photocatalysis has displayed promising results when using metal nanoparticles and metal oxides as photocatalysts, among which Ag [3], Au [4], SnO₂ [5],

* Correspondence to: Facultad de Ingeniería, Arquitectura y Diseño-Universidad Autónoma de Baja California, C.P. 22860 Ensenada, BC, México.

** Corresponding author.

E-mail addresses: pluque@uabc.edu.mx (P.A. Luque), carlos.sr@mochis.tecnm.mx (C.A. Soto-Robles).

<https://doi.org/10.1016/j.ijleo.2022.168937>

Received 10 September 2021; Received in revised form 29 December 2021; Accepted 17 March 2022

Available online 21 March 2022

0030-4026/© 2022 Elsevier GmbH. All rights reserved.

TiO₂ [6] and ZnO [7] nanoparticles stand out in the degradation of anionic and cationic dyes, as is the case of Methyl Orange (MO), Erichrome Black T (EBT), Congo Red (CR), Methyl Red, Methylene Blue (MB), Rhodamine B (RhB), Malachite Green (MG) and others [8]. ZnO NPs are the most sought after for these applications due to their chemical stability, non-toxicity, thermal stability and considerable efficiency in the degradation of organic contaminants as opposed to other semiconductors [9,10]. For the synthesis of this material, the path of green synthesis has been explored with aqueous plant extracts being used as reducing and stabilizing agents for NP growth control; by using this type of techniques, the less environmentally friendly, costly, chemical and physical methods have been replaced [11]. Green synthesis has been implemented previously for ZnO NPs synthesis, some of the extracts used have been: *Ruellia tuberosa* [12], *Dysphania ambrosioides* [13], *Azadirachta indica*, *Cymbopogon citratus* [14], *Eriobotria japonica* [15], *Acacia concinna* [16] and *Swertia chirayita* [17], to mention a few. Band gap size is one of the main characteristics of semiconductors, it is defined as the energy width between the valence band and the conduction band. For ZnO, this property has a value that borders on 3.37 eV. Some authors that have used natural extracts synthesized ZnO NPs for dye degradation, have reported Band gap values between 3.02 and 3.63, as is shown in Table 1.

The use of *Origanum vulgare* in green synthesis has already been explored for Au [28,29], Ag [30,31], Pd [32,33] and TiO₂ [34,35] NPs with different applications as is depicted in Fig. 1. *Origanum vulgare* is considered a potential reducing and stabilizing agent within the synthesis of this type of materials due to its phytochemical content. To our knowledge, there is no record to date concerning the synthesis of ZnO NPs using different concentrations of *Origanum vulgare* extract and how these affect their properties, mainly with regards to the Band gap and photocatalytic activity in RhB degradation. Hence, this is the first research where the effect of different *Origanum vulgare* extract concentrations in the green synthesis of ZnO NPs is studied, their properties, and application in RhB degradation.

2. Experimental

2.1. Extract preparation

The aim of this process is to obtain extracts with three different concentrations as clean as possible from *Origanum vulgare* solid residues. The concentrations of the *Origanum vulgare* extracts are 0.1%, 0.5% and 4% (% weight-volume) in aqueous medium. In this process for extracting the phytochemical agents, the different concentrations are prepared and shaken for two hours, next, they are placed in a water bath at 60 °C during an hour, and strained through a No. 4 Whatman filter. The obtained extracts are stored in refrigeration without light contact and used within a time frame no greater than 12 h for the ZnO NPs synthesis.

2.2. ZnO NPs synthesis

The final products of this procedure were the ZnO NPs samples that were labeled as follows: ZnO-OV-0.1%, ZnO-OV-0.5% and ZnO-OV-4%, which corresponded to the 0.1%, 0.5% and 4% extracts, respectively, used as stabilizing agents in the process. They were synthesized like so: firstly, 2 g of zinc nitrate (Zn(NO₃)₂ * 6 H₂O), as the Zn source, were added onto 42 mL of the obtained *Origanum vulgare* extracts and shaken until the precursor was completely dissolved. Subsequently, the samples were placed in a water bath at 60 °C until a paste-like consistency was visible and calcined at 400 °C for 60 min to obtain a dry, white powder, resulting these to be the ZnO NPs.

2.3. Characterization

Once the materials are obtained, it is important to know and determine their properties, therefore, the ZnO NPs were subjected to various techniques to elucidate some of them. To pinpoint the functional groups present in each of the samples, Fourier-Transform Infrared Spectroscopy (FTIR) was implemented; to examine the crystalline structure and phase of our materials, X-Ray Diffraction (XRD) was performed; likewise, X-Ray Photoelectron Spectrometry (XPS) was executed to confirm the chemical composition and to

Table 1
Band gap values of ZnO NPs synthesized using extracts.

Extract	Dye	Radiation	Band gap	Ref.
<i>Moringa oleifera</i>	–	–	With flowers 3.12 With seeds 3.18 Leaves 3.25	[18]
<i>Opuntia humifusa</i>	–	–	3.28 eV	[19]
<i>Alchemilla vulgaris</i>	Rhodamine B	Solar radiation	3.27 eV	[20]
Jujube fruit	Methylene Blue (MB) and Eriochrome Black-T (EBT)	Solar radiation	3.06 eV	[21]
<i>Syzygium cumini</i>	Methylene Blue (MB)	Solar radiation	3.32 eV	[22]
<i>Pithecellobium dulce peel</i>	Methylene Blue (MB)	Lamp (photoreactor)	3.14 eV	[23]
<i>Aloe vera</i>	–	–	range of 3.02–3.09 eV	[24]
<i>Vitis labruska</i>	Methylene Blue (MB)	Lamp	3.26 eV	[25]
<i>Artocarpus gomezianus</i>	Methylene Blue (MB)	Sun light and UV light	3.3 eV	[26]
<i>Euphorbia jatropa</i>	–	–	3.63	[27]



Fig. 1. Diagram of metal and metal oxide NPs synthesized using *Origanum vulgare* extracts and their applications.

establish if ZnO was truly being dealt with; High-Resolution Transmission Electron Microscopy (HR-TEM) allowed to probe and determine size, shape, and structure. The ZnO NPs were also characterized for photoluminescence. Furthermore, the Band gap was determined by ultraviolet-visible spectroscopy (UV-Vis) as well as the catalytic activity in RhB degradation.

2.4. Photocatalytic activity

To measure the photocatalytic activity, two tests were carried out: one in UV-light radiance and the other in solar light. For these analyses, 50 mg of ZnO NPs were added onto 50 mL of RhB, 15 ppm. This solution was shaken for 30 min without any light and subsequently irradiated with an ultraviolet light lamp at 10 W potency and a dose of 18 mJ/ cm², or solar light, accordingly. To perform the assays and measurements of RhB concentration in a UV-vis spectrophotometer, 2 mL aliquots were taken every 30 min for 180 min and analyzed at 664 nm maximum absorbance.

The Eq. (1) that describes the percentage of RhB degradation (%D) is the following:

$$\%D = ((C_0 - C_t) / C_0) * 100 \quad (1)$$

Where C₀ is the initial concentration of RhB and C_t is the concentration of RhB at different time intervals.

3. Results and discussion

3.1. FTIR

In Fig. 2, ZnO NPs can be observed as characterized by FTIR from 4500 a 300 cm⁻¹, where the 1399 cm⁻¹ (O-H) and 871 cm⁻¹ (aromatic C-H) bands are apparent [36]. These signals are attributed to the functional groups existing in the organic components contained within the *Origanum vulgare* extracts, which increase in intensity as the extract concentration (weight-volume) is risen

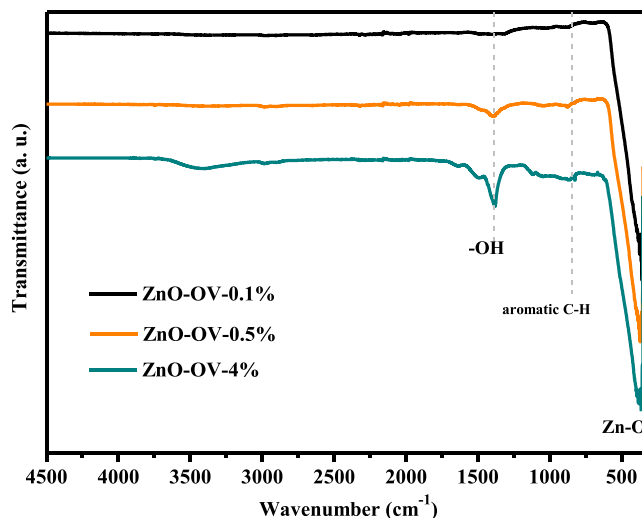


Fig. 2. FTIR spectra of the ZnO samples.

during ZnO NPs synthesis. The characteristic band of the Zn-O bond that allows us to confirm that our material is zinc oxide is found at 384 cm^{-1} , corresponding to metal-oxide bonds [10].

3.2. XRD and structural study

The X-ray diffraction patterns of the ZnO NPs samples from Fig. 3 allow us to estimate the crystallite size of the synthesized materials through the Scherrer formula, which is defined as:

$$\tau = K\lambda / \beta \cos\theta \quad (2)$$

where: τ , is the crystallite average size; K , a unitless value of 0.9; λ , the wavelength of the X-rays; β , the full width at half maximum intensity; and θ , is Bragg's angle [37].

The crystallite sizes calculated from the XRD diffractograms were 37.3, 35.6 and 8.4 nm, for ZnO-OV-0.1%, ZnO-OV-0.5% and ZnO-OV-4%, respectively. In Fig. 3 various peaks that correspond to the hexagonal structure of the Wurtzite crystalline phase of ZnO NPs (JCPDS: 36–1451) can be seen. The signals are located at 31.79° , 34.44° , 36.27° , 47.55° , 56.61° , 62.85° and 67.91° and indexed to the crystal planes (100), (002), (101), (102), (110), (103) and (112) [38]. In order to make the most out of the results obtained by XRD, these were subjected to a Rietveld refinement methodology by the High Score Plus software. Rietveld refinement is used to find refined structural parameters such as cell volume, lattice, density, etc. and microstructural parameters like microdeformation [39]. Table 2 shows the parameters refined parameters. The results reveal that the samples have a hexagonal structure that belongs to the P63mc spatial group and the values of the lattice parameters match with those reported in literature (Crystallographic card JCPDS 36–1451). The quality of the adjustment is derived from some reliability indexes such as R_{wp} , R_{exp} , R_p , and GoF. GoF is calculated by Eq. (3).

$$\text{GoF} = R_{wp} / R_{exp} \quad (3)$$

where R_{wp} , and R_{exp} are the weighted profile reliability parameter and expected R factor, respectively. Conversely, R_p is related to the crystalline structure [40].

The GoF values found for the three samples fall within the range of values reported in literature, which confirms that the refinement parameters are determined with greater precision [41–43].

3.3. Morphology study

In Fig. 4, the TEM, HR-TEM and EDX analysis can be seen for ZnO-OV-0.1%, ZnO-OV-0.5% and ZnO-OV-4%. All of the samples hold irregular shapes, the majority of which are oval with certain spherical tendencies. As we increase the extract synthesis concentration, a smaller nanoparticle size can be appreciated, that is, the amount of extract has a direct influence on morphology, especially over the shape of the ZnO nanostructures as is observed in TEM Fig. 4 (A, D and G) and in the HR-TEM micrographs that are provided in Fig. 4 (B, E and H). The ZnO-OV-4% sample has a tendency to form NPs that are more homogeneous in shape and size, it is as well the one that presented smaller sizes mainly owing to the quantity of bioactive compounds present in the extract which function as stabilizing

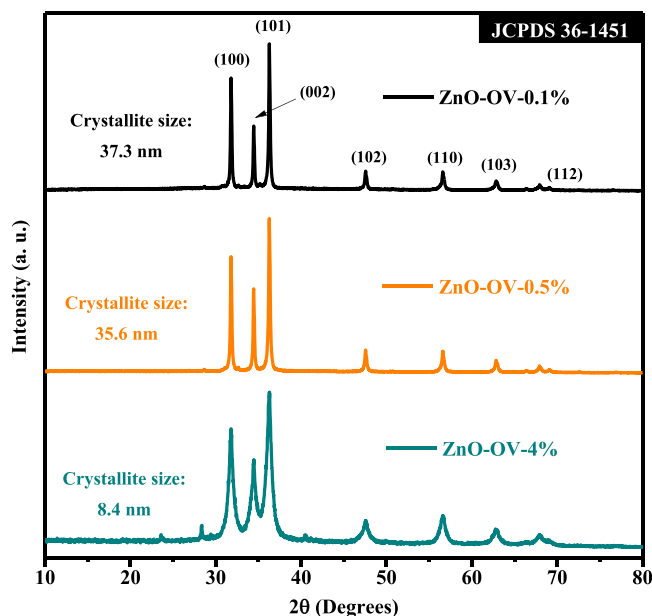


Fig. 3. XRD patterns of the ZnO NPs.

Table 2
Results obtained by Rietveld refinement.

Material	Crystalstructure	Spacegroup	Latticeparameter	ϵ (%)	Density (g/cm ³)	Cellvolume (Å ³)	R factors (%)
0.1%	Hexagonal	P 63 m c	a = 3.2554 Å b = 3.2554 Å c = 5.2157 Å $\alpha = 90^\circ$ $\beta = 90^\circ$ $\gamma = 120^\circ$	0.232	5.6450	47.87008	R _{exp} = 7.36890 R _p = 21.78363 R _{wpp} = 28.04980 GoF = 3.80651
0.5%	Hexagonal	P 63 m c	a = 3.2544 Å b = 3.2544 Å c = 5.2135 Å $\alpha = 90^\circ$ $\beta = 90^\circ$ $\gamma = 120^\circ$	0.230	5.6512	47.81812	R _{exp} = 8.06965 R _p = 26.51287 R _{wpp} = 33.53693 GoF = 4.15593
4%	Hexagonal	P 63 m c	a = 3.257 Å b = 3.257 Å c = 5.219 Å $\alpha = 90^\circ$ $\beta = 90^\circ$ $\gamma = 120^\circ$	0.877	5.6360	47.94669	R _{exp} = 8.09120 R _p = 17.39183 R _{wpp} = 22.43976 GoF = 2.77335

agents, preventing the further growth of nanoparticles [44], which indicates that they provide greater stability during the synthesis process. The size distribution can be analyzed in insets Fig. 4 (A, D and G). The sizes that were found correlate to those calculated by the Scherrer equation in the XRD assay. The more homogeneous nanoparticles size distribution is considered to be that of the ZnO-OV-4% sample whose sizes fall mainly between 8 and 10 nm. For ZnO-OV-0.1% and ZnO-OV-0.5%, there is greater variation in the sizes, but it can as well be appreciated that the smaller the amount of extract used, the greater the particle sizes obtained are. Based on the HR-TEM analysis, Fig. 4 (B, E and H), of the three samples, the lattice fringe distance was found to be 0.28 nm, which belongs to the (100) plane. This plane is characteristic of the Wurtzite phase of ZnO as reported in several publications [45,46], which proves the obtaining of this phase and is in accord with the planes acquired through XRD for the three quantities of extract used. For a better assessment of the samples, EDX analyses were performed to determine the elemental composition of the synthesized nanoparticles as shown in Fig. 4 (C, F, and I) for ZnO-OV-0.1%, ZnO-OV-0.5%, and ZnO-OV-4%, respectively. All of the nanoparticles exhibited the presence of Zn, O, and the elements that compose the grid used as support during the analysis, which demonstrates and confirms the synthesis of ZnO nanoparticles [47].

3.4. X-ray photoelectron spectrometry (XPS)

In Fig. 5, the survey scans are observed of the ZnO NPs synthesized using *Origanum vulgare* extracts (ZnO-OV-0.1%, ZnO-OV-0.5% and ZnO-OV-4%). The analyses were calibrated considering as reference the main peak of C1s (284.5 eV) [48]. In these survey scans, only the main peaks belonging to the elements O (O1s) and Zn (Zn2p_{1/2} y Zn2p_{3/2}) were found, which are unique to ZnO NPs [49], indicating that the material was obtained satisfactorily whilst changing the extract concentrations. Similarly, for the three cases, the main peak of C (C1s) was found, this signal corresponds to carbon from the organic matter present in the molecules of the *Origanum vulgare* extracts used in the green synthesis of the ZnO NPs, in accordance with the results obtained by FTIR analyses, where the presence of C was identified in different functional groups, aside from the ZnO NPs (Fig. 2).

In the high resolution XPS analysis, the main peaks of O1s and Zn2p were assayed, which are portrayed in Fig. 6. For the case of O1s (Fig. 6A), the peak was found in its characteristic position at 531 eV [50] without there being any variation for ZnO-OV-0.1%, ZnO-OV-0.5%, or ZnO-OV-4%. This was proven by the analysis of the Zn2p peak (Fig. 6B), where the characteristic doublet was found, that is the Zn2p_{1/2} and Zn2p_{3/2} peak located at 1044.5 and 1022.5 eV, respectively, as has been reported in other investigations [51], furthermore, it can be seen that there exists a difference in energy of 23 eV between Zn2p_{1/2} and Zn2p_{3/2}, which is proper of Zn²⁺ species that belong to ZnO NPs [52], ratifying the formation of the Zn-O bond.

3.5. Band gap

The samples were analyzed by UV-vis spectroscopy, where absorbance signals were observed between 350 and 400 nm, these varied according to the amount of extract involved in the synthesis of the ZnO NPs; they were also used for determining the Band gap following the Tauc model [53]. The acquired Band gap values were 2.29, 2.77 and 2.94 eV for ZnO-OV-0.1%, ZnO-OV-0.5% and ZnO-OV-4%, respectively, as can be seen in Fig. 7. These values are similar to those previously published for ZnO nanoparticles [54].

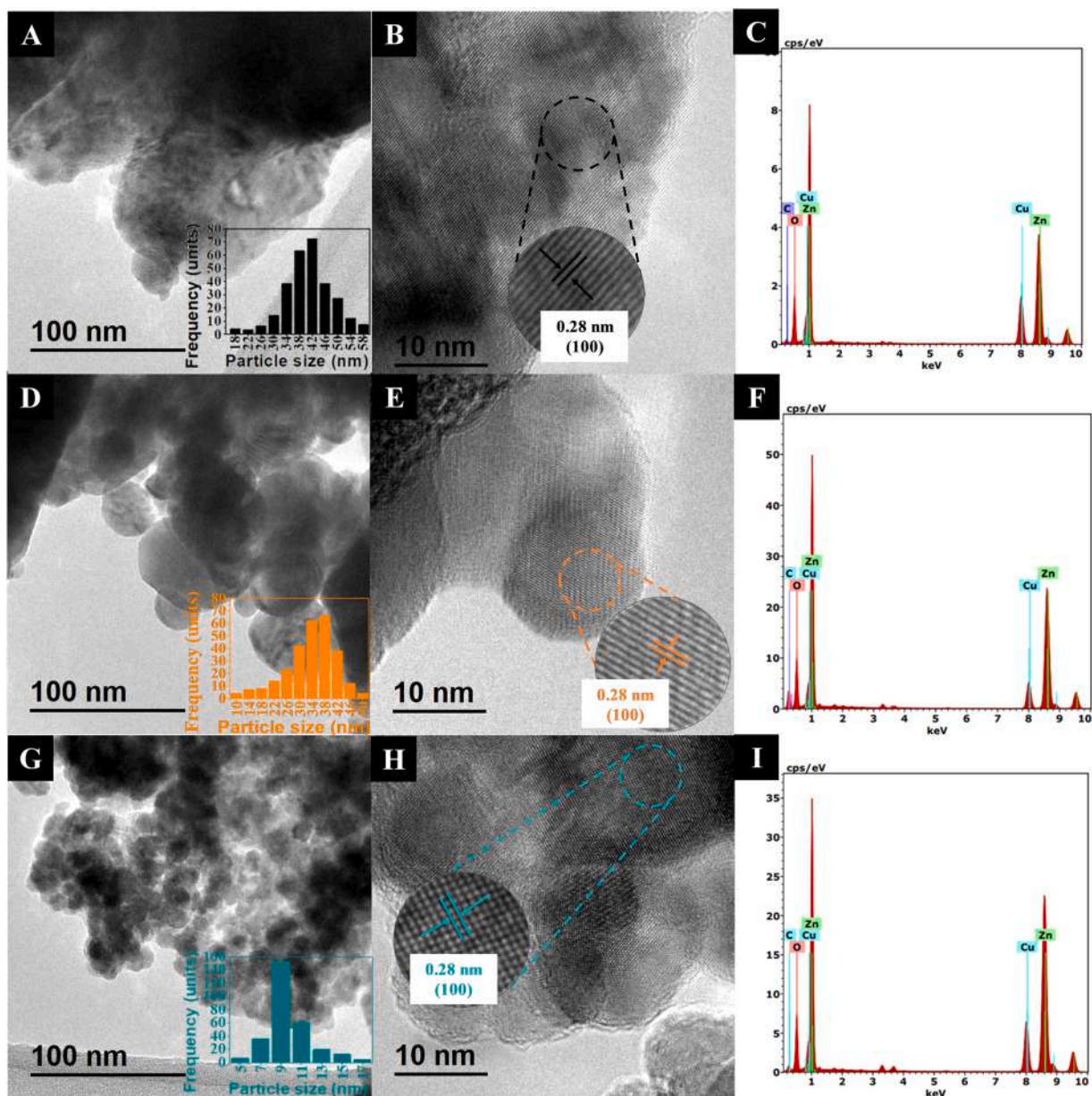


Fig. 4. Morphology of ZnO NPs through HR-TEM A and B) ZnO-OV-0.1%, D and E) ZnO-OV-0.5% and G and H) ZnO-OV-4%, where inset show the size distribution and EDX analysis of C) ZnO-OV-0.1%, F) ZnO-OV-0.5% and I) ZnO-OV-4%.

3.6. Photoluminescence

Fig. 8 depicts the emission spectra of the ZnO NPs (ZnO-OV-0.1%, ZnO-OV-0.5% and ZnO-OV-4%) excited at 320 nm. The PL spectrum shows a weak UV emission band and a broad visible emission band that covers almost all the visible region, confirming that they indeed are ZnO NPs of spherical shape and nanometric scale. In the emission spectra (Fig. 8), there is a sharp peak centered between 400 and 420 nm (visible region) in all samples. The main emission peaks in the visible region are centered between 480 and 500 nm (blue region); also, weak signals and a slope starting at 495 nm can be appreciated, which correspond to the green region. Additionally, the PL graphic study shows that as the concentration of *Origanum vulgare* increases, the emission peak at 590 nm (orange-yellow region) becomes more prominent and the signal approaches 700 nm that corresponds to the red region [55].

3.7. Catalytic activity

The synthesized ZnO NPs were used for the photocatalytic degradation of RhB in UV radiation and solar radiation. During the

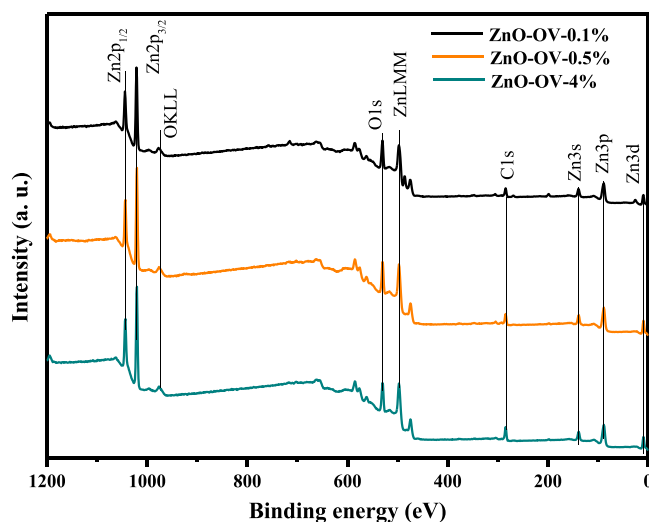


Fig. 5. XPS spectra of ZnO Nps.

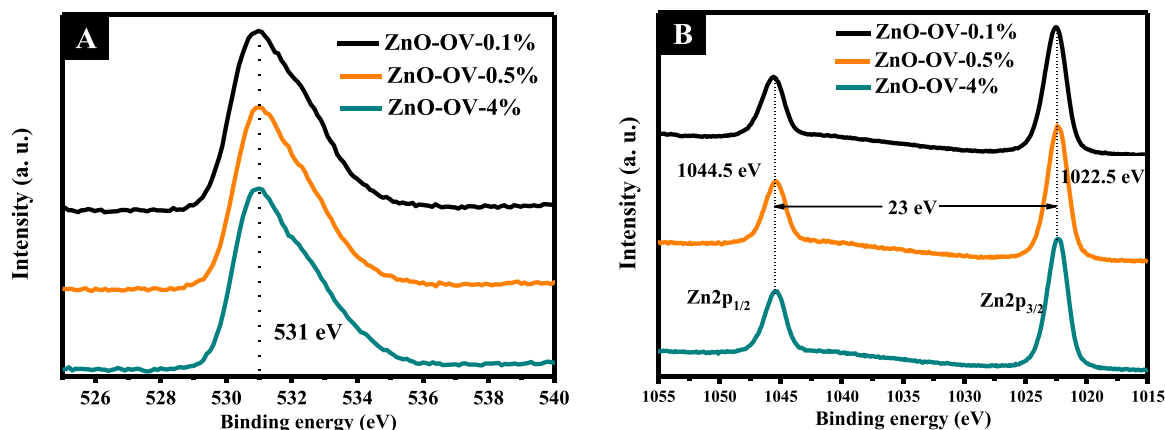


Fig. 6. High resolution analyses of the main peaks of (a) O1s and (b) Zn2p of ZnO NPs.

preliminary experiments, the samples were shaken in darkness for 30 min to discard RhB adsorption effects; whereas in the assays in UV radiation, the ZnO-OV-0.1%, ZnO-OV-0.5% and ZnO-OV-4% samples adsorbed only 1% (Fig. 9a), owing to the low affinity between RhB and the ZnO NPs [56]. In the solar light experiment, no adsorption effect was found (Fig. 9c), proving the nonexistent affinity of the nanoparticles for the dye. Once equilibrium was reached, the UV lamp was switched on, for the case of UV radiation, and the samples were placed in the sun, for the case of solar radiation; the results can be observed in Fig. 9.

In the UV-light set up, good yields were obtained for all three samples; it can be seen that over the course of time, Rhodamine B concentration decreased until degradation was accomplished [57]. The best sample was ZnO-OV-4%, which achieved 93% degradation at the 180 min mark, showing photocatalytic efficiency improvement in comparison to other investigations reported previously [58]. For the test in solar light, a behavior similar to that in UV radiation was seen, where ZnO-OV-0.1%, ZnO-OV-0.5% and ZnO-OV-4% conveyed very good yields considering that ZnO commercial nanoparticles show very low efficiency in solar light due to the fact that this type of radiation does not possess enough energy to excite them [59]. Our results revealed that the best degradation outcomes were depicted by the ZnO-OV-0.5% and ZnO-OV-4% samples, achieving 88% degradation within 80 min and 94.24% in 100 min, this is attributed to the organic molecules from the oregano extract that remain on the nanoparticles after the biosynthesis process (see FTIR and XPS). These molecules act as photosensitizers that induce the nanoparticles to be excited with less energy (see Band gap section) [60], say visible light. Through the performed experiments, it was proven that the biosynthesized nanoparticles exhibit good efficiency in photocatalytic degradation of Rhodamine B dye. Furthermore, these results helped to successfully obtain the values of the degradation rate constants (k), which relate to the photocatalytic speed in the experiments. For the assays in UV radiation (Fig. 9b), a k growth tendency is made evident as the amount of extract used increases, where the best result was exhibited by ZnO-OV-2% (3.77×10^{-2}), whereas in the solar light experiments (Fig. 9d), the greatest k value was exhibited by ZnO-OV-4% (1.38×10^{-2}). The k values depicted in this work are greater than those reported in literature [61]. The improvement in photocatalytic

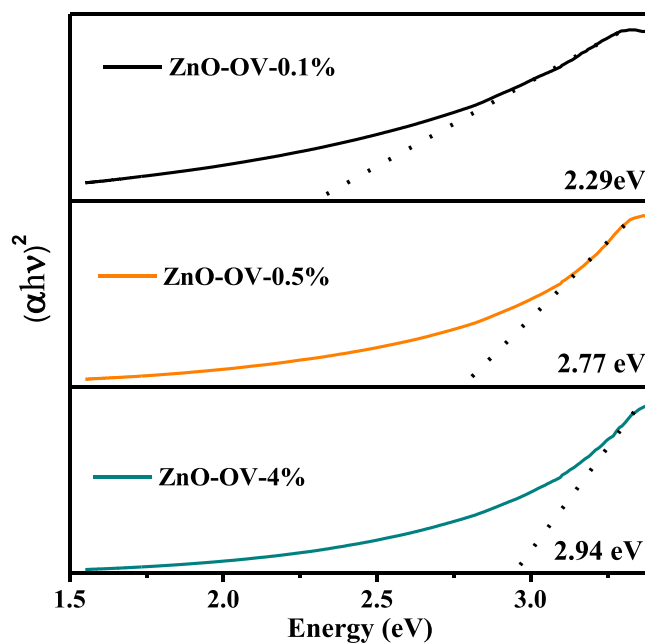


Fig. 7. Band gap of the ZnO NPs.

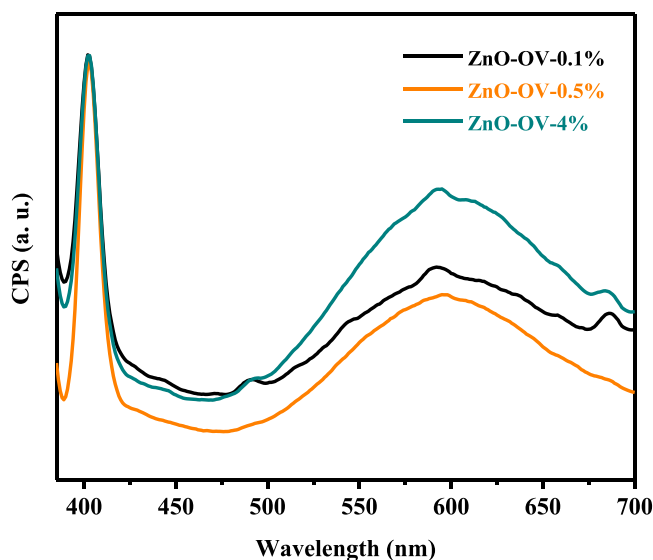


Fig. 8. Photoluminescence (PL) spectrum of ZnO.

performance of the biosynthesized nanoparticles was confirmed by the Turn Over Number (TON) and Turn Over Frequency (TOF) values, which define the sum of catalytic cycles that are carried out on each active site per time unit [62]. The calculated TON and TOF results are disclosed in Table 3; it is evident there is a tendency to render greater and better results as the amount of extract used during biosynthesis increases; the highest value was portrayed by ZnO-OV-4% in UV radiation (1.40×10^{-3}) as well as in solar radiation (1.32×10^{-3}).

3.7.1. Degradation mechanism

The degradation mechanism for Rhodamine B is proposed as is disclosed in Fig. 10. The degradation process begins when photons from the radiation source are absorbed by the surface of ZnO nanoparticles causing excitation of valence band (VB) electrons, prompting their transportation to the conduction band (CB) [63], leaving a hole in the VB. This process results in the emergence of electron-hole pairs [64]. The excited CB electrons interact with molecular oxygen (O_2) to generate superoxide radicals (O_2^-); similarly,

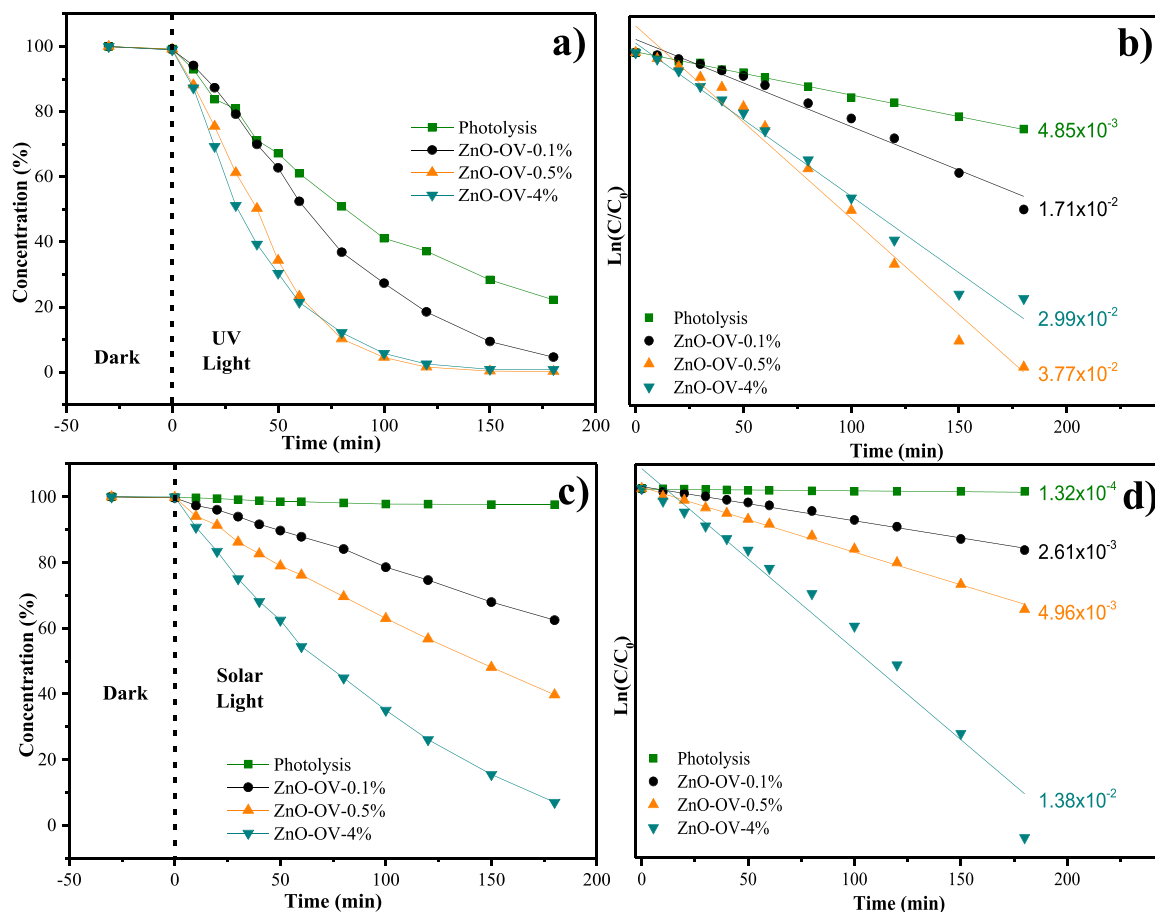


Fig. 9. Photocatalytic degradation of Rhodamine B in UV light (a) degradation rate constants in UV light, (b) photocatalytic degradation of Rhodamine B in solar light (c) and (d) degradation rate constants in solar light.

Table 3

Turn over frequency results.

	Material	TON	TOF (min^{-1})
Solar Light	Photolysis	6.04×10^{-3}	3.36×10^{-5}
	ZnO-OV-0.1%	9.57×10^{-2}	5.32×10^{-4}
	ZnO-OV-0.5%	15.40×10^{-2}	8.56×10^{-4}
	ZnO-OV-4%	23.70×10^{-2}	1.32×10^{-3}
UV Light	Photolysis	19.83×10^{-2}	1.10×10^{-3}
	ZnO-OV-0.1%	24.31×10^{-2}	1.35×10^{-3}
	ZnO-OV-0.5%	25.43×10^{-2}	1.41×10^{-3}
	ZnO-OV-4%	25.28×10^{-2}	1.40×10^{-3}

the VB holes generate hydroxyl radicals (OH^\cdot) owing to their contact with water molecules (H_2O). The O_2^\cdot and OH^\cdot species have a high oxidative power and are responsible for leading the degradation of RhB. Proceeding down the mechanism, O_2^\cdot and OH^\cdot react with the RhB molecules accomplishing their degradation through three decomposition stages: (I) In the first stage of the process, the RhB molecule's chromophores are broken off by effect of the oxidative species attack against the central carbon of the molecule, oxidating it and generating an intermediary species of lower molecular weight [65]. (II) In the second stage, the rings of the intermediary species are cleaved by attack of the oxidative species producing small, open-ring compounds [66]. (III) In the third and last stage, the compounds generated after the opening of the rings are degraded to final products such as mineralized compounds, H_2O , and CO_2 [67].

4. Conclusions

In this work, it is important to highlight the direct effect the concentration of the aqueous extracts of *Origanum vulgare* has in the synthesis of ZnO NPs, resulting in the modification of the Band gap values in line with the amount of extract used. As a consequence,

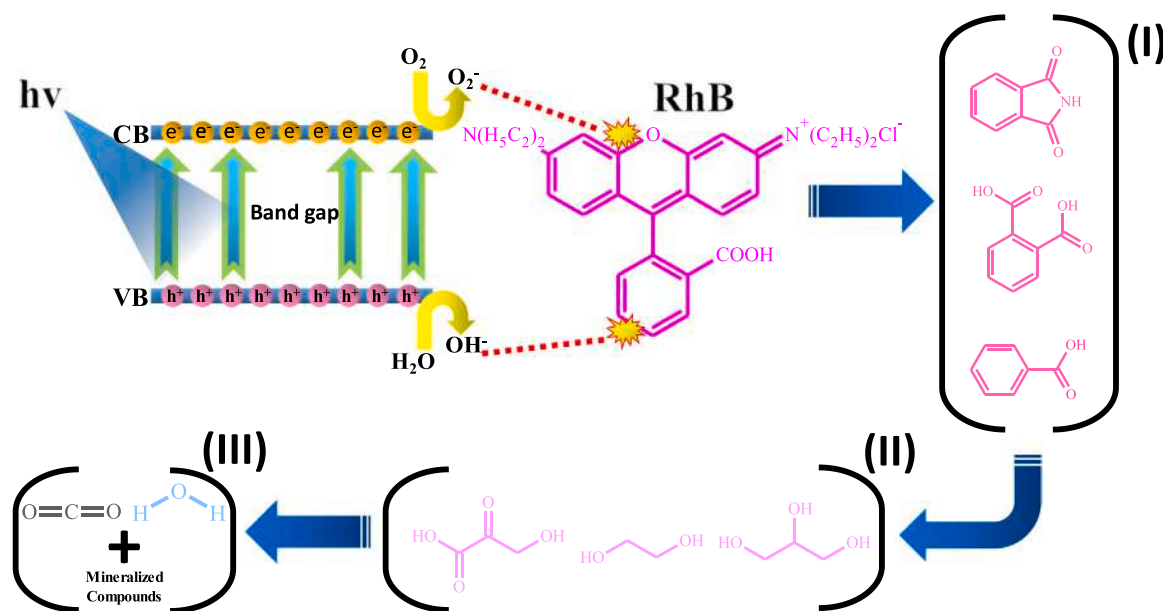


Fig. 10. Proposed mechanism for the degradation of RhB.

the latter impacts the RhB degradation yield by virtue of the ZnO NPs photocatalyst used. The concentrations of *Origanum vulgare* extract used in the syntheses were 0.1%, 0.5% and 4% (% weight-volume). The Band gap values are 2.94, 2.77 and 2.29 eV for ZnO-OV-0.1%, ZnO-OV-0.5% and ZnO-OV-4%, respectively; these values increase proportionately to the rise in extract concentration. These materials exhibit good photocatalytic activity; although, the ZnO NPs sample that was synthesized using 4% extract depicted the best results, degrading 94.24% of RhB in 100 min in UV light and 93% within 180 min in solar light. As mentioned, the extract concentration used not only modifies the Band gap values of the ZnO NPs, but also varies their size and size distribution, ranging from 37 to 8 nm, the smallest sizes resulting from highest concentration. Moreover, the ZnO NPs morphology holds semicircular shapes.

Declaration of Competing Interest

The authors report no declarations of interest.

Acknowledgments

Authors thank to CONACYT for financial support (Grant No. 295075 Infrastructure, Grant No. 4940 National Problems), to the Universidad Autónoma de Baja California for project number 676, to PRODEP with official number 511-6/2020-9926, and we gratefully acknowledge the use of TEM facilities at the TEM Laboratory of Universidad de Sonora.

References

- [1] R. Dobrucka, J. Długaszewska, Biosynthesis and antibacterial activity of ZnO nanoparticles using *Trifolium pratense* flower extract, *Saudi J. Biol. Sci.* 23 (2016) 517–523.
- [2] G. Yashni, A. Al-Gheethi, R.M.S.R. Mohamed, N.V. Dai-Viet, A.A. Al-Kahtani, M. Al-Sahari, S. Alkhadher, Bio-inspired ZnO NPs synthesized from *Citrus sinensis* peels extract for Congo red removal from textile wastewater via photocatalysis: Optimization, mechanisms, techno-economic analysis, *Chemosphere* 281 (2021) 130661–130672.
- [3] M. Aravind, A. Ahmad, I. Ahmad, M. Amalanathan, K. Naseem, S.M.M. Mary, M. Zuber, Critical green routing synthesis of silver NPs using Jasmine flower extract for biological activities and photocatalytic degradation of methylene blue, *J. Environ. Chem. Eng.* 9 (2021) 104877–104885.
- [4] D. Baruah, M. Goswami, R.N.S. Yadav, A. Yadav, A.M. Das, Biogenic synthesis of gold nanoparticles and their application in photocatalytic degradation of toxic dyes, *J. Photochem. Photobiol. B* 186 (2018) 51–58.
- [5] J. Singh, H. Kaur, D. Kukkar, V.K. Mukamia, S. Kumar, M. Rawat, Green synthesis of SnO₂ NPs for solar light induced photocatalytic applications, *Mater. Res. Express* 6 (2019) 115007–115014.
- [6] G. Nabi, Q.U. Ain, M.B. Tahir, K. Nadeem Riaz, T. Iqbal, M. Rafique, M. Rizwan, Green synthesis of TiO₂ nanoparticles using lemon peel extract: their optical and photocatalytic properties, *Int. J. Environ. Anal. Chem.* 1 (2020) 1–9.
- [7] L.A. Chanu, W.J. Singh, K.J. Singh, K.N. Devi, Effect of operational parameters on the photocatalytic degradation of Methylene blue dye solution using manganese doped ZnO nanoparticles, *Results Phys.* 12 (2019) 1230–1237.
- [8] P.C. Nagajyothi, S.V. Prabhakar Vattikuti, K.C. Devarayapalli, K. Yoo, J. Shim, T.V.M. Sreekanth, Green synthesis: photocatalytic degradation of textile dyes using metal and metal oxide nanoparticles-latest trends and advancements, *Crit. Rev. Environ. Sci. Technol.* 50 (2020) 2617–2723.
- [9] K. Qi, B. Cheng, J. Yu, W. Ho, Review on the improvement of the photocatalytic and antibacterial activities of ZnO, *J. Alloy. Compd.* 727 (2017) 792–820.
- [10] J.K. Park, E.J. Rupa, M.H. Arif, J.F. Li, G. Anandapadmanaban, J.P. Kang, S.C. Kang, Synthesis of zinc oxide nanoparticles from *Gynostemma pentaphyllum* extracts and assessment of photocatalytic properties through malachite green dye decolorization under UV illumination-A green approach, *Optik* 239 (2021) 166249–166259.

- [11] S. Ahmed, S.A. Chaudhry, S. Ikram, A review on biogenic synthesis of ZnO nanoparticles using plant extracts and microbes: a prospect towards green chemistry, *J. Photochem. Photobiol. B* 166 (2017) 272–284.
- [12] S. Vasantharaj, S. Sathiyavimal, P. Senthilkumar, V.N. Kalpana, G. Rajalakshmi, M. Alselhi, A. Pugazhendhi, Enhanced photocatalytic degradation of water pollutants using bio-green synthesis of zinc oxide nanoparticles (ZnO NPs), *J. Environ. Chem. Eng.* 9 (2021) 105772–105779.
- [13] R. Álvarez-Chimal, V.I. García-Pérez, M.A. Álvarez-Pérez, J.A. Arenas-Alatorre, Green synthesis of ZnO nanoparticles using a *Dysphania ambrosioides* extract. Structural characterization and antibacterial properties, *Mater. Sci. Eng. C* 118 (2021) 111540–111542.
- [14] T. Zaheer, M. Imran, K. Pal, M.S. Sajid, R.Z. Abbas, A.I. Aqib, S. ur Rahman, Synthesis, characterization and acaricidal activity of green-mediated ZnO nanoparticles against *Hyalomma* ticks, *J. Mol. Struct.* 1227 (2021) 129652–129659.
- [15] M. Shabaani, S. Rahaiee, M. Zare, S.M. Jafari, Green synthesis of ZnO nanoparticles using loquat seed extract; Biological functions and photocatalytic degradation properties, *LWT* 134 (2020) 110133–110142.
- [16] P. Palai, S. Muduli, B. Priyadarshini, T.R. Sahoo, A facile green synthesis of ZnO nanoparticles and its adsorptive removal of Congo red dye from aqueous solution, *Mater. Today.: Proc.* 38 (2021) 2445–2451.
- [17] R. Saha, K. Subramani, S. Sikdar, K. Fatma, S. Rangaraj, Effects of processing parameters on green synthesised ZnO nanoparticles using stem extract of *Swertia chirayita*, *Biocatal. Agric. Biotechnol.* 33 (2021) 101968–101978.
- [18] I. Ngom, B.D. Ngom, J. Sackey, S. Khamlich, Biosynthesis of zinc oxide nanoparticles using extracts of *Moringa oleifera*: Structural & optical properties, *Mater. Today.: Proc.* 36 (2021) 526–533.
- [19] M. Chennimalai, V. Vijayalakshmi, T.S. Senthil, N. Sivakumar, One-step green synthesis of ZnO nanoparticles using *Opuntia humifusa* fruit extract and their antibacterial activities, *Mater. Today.: Proc.* 47 (2021) 1842–1846.
- [20] S. Rajendrachari, P. Taslimi, A.C. Karaoglanli, O. Uzun, E. Alp, G.K. Jayaprakash, Photocatalytic degradation of Rhodamine B (RhB) dye in waste water and enzymatic inhibition study using cauliflower shaped ZnO nanoparticles synthesized by a novel One-pot green synthesis method, *Arab. J. Chem.* 14 (2021) 103180–103192.
- [21] M. Golmohammadi, M. Honarmand, S. Ghanbari, A green approach to synthesis of ZnO nanoparticles using jujube fruit extract and their application in photocatalytic degradation of organic dyes, *Spectrochim. Acta A Mol. Biomol. Spectrosc.* 229 (2020) 117961–117969.
- [22] H. Sadiq, F. Sher, S. Sehar, E.C. Lima, S. Zhang, H.M. Iqbal, M. Nuhaniović, Green synthesis of ZnO nanoparticles from *Syzygium cumini* leaves extract with robust photocatalysis applications, *J. Mol. Struct.* 335 (2021) 116567–116575.
- [23] G. Madhumitha, J. Fowsiya, N. Gupta, A. Kumar, M. Singh, Green synthesis, characterization and antifungal and photocatalytic activity of *Pithecellobium dulce* peel mediated ZnO nanoparticles, *J. Phys. Chem. Solids* 127 (2019) 43–51.
- [24] N.H. Deepthi, A. Amrutha, H. Nagabhushana, R.B. Basavaraj, Facile green approach for the synthesis of ZnO Superstructures: Their structural and photometric properties, *Mater. Today.: Proc.* 5 (2018) 20803–20810.
- [25] G. Nagaraju, H. Nagabhushana, D. Suresh, C. Anupama, G.K. Raghu, S.C. Sharma, *Vitis labruska* skin extract assisted green synthesis of ZnO super structures for multifunctional applications, *Ceram. Int.* 43 (2017) 11656–11667.
- [26] D. Suresh, R.M. Shobharani, P.C. Nethravathi, M.P. Kumar, H. Nagabhushana, S.C. Sharma, *Artocarpus gomezianus* aided green synthesis of ZnO nanoparticles: luminescence, photocatalytic and antioxidant properties, *Spectrochim. Acta A Mol. Biomol. Spectrosc.* 141 (2015) 128–134.
- [27] M.S. Geetha, H. Nagabhushana, H.N. Shivananjai, Green mediated synthesis and characterization of ZnO nanoparticles using *Euphorbia jatropha* latex as reducing agent, *J. Sci.: Adv. Mater. Devices* 1 (2016) 301–310.
- [28] D. Benedec, I. Oniga, F. Cuius, B. Sevastre, G. Stiuftuc, M. Duma, C.M. Lucaci, *Origanum vulgare* mediated green synthesis of biocompatible gold nanoparticles simultaneously possessing plasmonic, antioxidant and antimicrobial properties, *Int. J. Nanomed.* 13 (2018) 1041–1058.
- [29] M.S. Aguilar, F. Mares-Briones, S.E. Borjas-García, G. Rosas, Green Synthesis of Gold Nanoparticles Using *Origanum vulgare*, *Microsc. Microanal.* 25 (2019) 2378–2379.
- [30] N. Genc, Biosynthesis of silver nanoparticles using *Origanum onites* extract and investigation of their antioxidant activity, *Part. Sci. Technol.* 39 (2020) 562–568.
- [31] R. Sankar, A. Karthik, A. Prabu, S. Karthik, K.S. Shivashangari, V. Ravikumara, *Origanum vulgare* mediated biosynthesis of silver nanoparticles for its antibacterial and anticancer activity, *Colloids Surf. B Biointerfaces* 108 (2013) 80–84.
- [32] M.R. Shaikh, Z.J.Q. Ali, M. Khan, M. Kuniyil, M.E. Assal, H.Z. Alkhatlan, S.F. Adil, Green synthesis and characterization of palladium nanoparticles using *Origanum vulgare* L. extract and their catalytic activity, *Molecules* 22 (2017) 165–176.
- [33] N. Seyedi, K. Saidi, H. Sheibani, Green synthesis of Pd nanoparticles supported on magnetic graphene oxide by *Origanum vulgare* leaf plant extract: catalytic activity in the reduction of organic dyes and Suzuki–Miyaura cross-coupling reaction, *Catal. Lett.* 148 (2018) 277–288.
- [34] R. Sankar, R. Dhivya, K.S. Shivashangari, V. Ravikumara, Wound healing activity of *Origanum vulgare* engineered titanium dioxide nanoparticles in Wistar Albino rats, *J. Mater. Sci.: Mater. Med.* 25 (2014) 1701–1708.
- [35] M. Bahmani, A new method for promoting biogenic synthesis and reducing the size of titanium dioxide nanoparticles (TiO₂ NPs) synthesized by *Origanum vulgare*, *Plant Biotechnol. Persa* 1 (2019) 10–12.
- [36] T.U.D. Thi, T.T. Nguyen, Y.D. Thi, K.H.T. Thi, B.T. Phan, K.N. Pham, Green synthesis of ZnO nanoparticles using orange fruit peel extract for antibacterial activities, *RSC Adv.* 10 (2020) 23899–23907.
- [37] C.H.N. Van, H.K. Nguyen, H.Q. Huynh, H.A. Pham, T.M. Dinh, H.N. Luong, V.Q. Dang, Multi-modification of ZnO nanorods to enhance the visible absorption, *Adv. Nat. Sci.: Nanosci. Nanotechnol.* 11 (2020) 015002–015009.
- [38] K. Rambabu, G. Bharath, F. Banat, P.L. Show, Green synthesis of zinc oxide nanoparticles using *Phoenix dactylifera* waste as bioreductant for effective dye degradation and antibacterial performance in wastewater treatment, *J. Hazard. Mater.* 402 (2021) 123560–123571.
- [39] Y. Ando, T. Oku, Y. Ohishi, Rietveld refinement of crystal structure of perovskite CH₃NH₃Pb(Sb)I₃ solar cells, *Jpn. J. Appl. Phys.* 57 (2017), 02CE021–02CE025.
- [40] B. Maibam, S. Baruah, B.P. Singh, S. Kumar, Quantitative analysis of Fe/Co co-doped ZnO by Rietveld method, *Indian, J. Pure Appl. Phys.* 58 (2020) 673–677.
- [41] K. Pradeeswari, A. Venkatesan, P. Pandi, K. Karthik, K.V. Hari Krishna, R. Mohan, Kumar, Study on the electrochemical performance of ZnO nanoparticles synthesized via non-aqueous sol-gel route for supercapacitor applications, *Mater. Res. Express* 6 (2019), 105525.
- [42] P. Kumar, A.K. Yadav, A.G. Joshi, D. Bhattacharyya, S.N. Jha, P.C. Pandey, Influence of Li co-doping on structural property of sol-gel derived terbium doped zinc oxide nanoparticles, *Mater. Charact.* 142 (2018) 593–601.
- [43] M.I. Said, A.A.M. Aly, A.I. El-Said, A. Abou-Taleb, Controlled synthesis of ZnO nanoparticles from a Zn(II) coordination polymer: Structural characterization, optical properties and photocatalytic activity, *Appl. Organomet. Chem.* 34 (2020) e5858–e5872.
- [44] H. Agarwal, S. Venkat Kumar, S. Rajeshkumar, A review on green synthesis of zinc oxide nanoparticles -An eco-friendly approach, *Resour. Technol.* 3 (2017) 406–413.
- [45] R. Sankar Ganesh, E. Durgadevi, M. Navaneethan, V.L. Patil, S. Ponnusamy, C. Muthamizhchelvan, S. Kawasaki, P.S. Patil, Y. Hayakawa, Low temperature ammonia gas sensor based on Mn-doped ZnO nanoparticle decorated microspheres, *J. Alloy. Compd.* 721 (2017) 182–190.
- [46] Y. Song, S. Zhang, C. Zhang, Y. Yang, K. Lv, Raman Spectra and Microstructure of Zinc Oxide irradiated with Swift Heavy Ion, *Cryst* 9 (2019) 395–402.
- [47] M. Fakhar-e-Alam, S. Rahim, M. Atif, M. Hammad Aziz, M. Imran Malick, S.S.Z. Zaidi, R. Suleman, A. Majid, ZnO nanoparticles as drug delivery agent for photodynamic therapy, *Laser Phys. Lett.* 11 (2013) 25601–25607.
- [48] L.-H. Chen, A. Huang, Y.-R. Chen, C.-H. Chen, C.-C. Hsu, F.-Y. Tsai, K.-L. Tung, Omniphobic membranes for direct contact membrane distillation: Effective deposition of zinc oxide nanoparticles, *Desalination* 428 (2018) 255–263.
- [49] Y. Sun, Y. Zong, J. Feng, X. Li, F. Yan, Y. Lan, L. Zhang, Z. Ren, X. Zheng, Oxygen vacancies driven size-dependent d₀ room temperature ferromagnetism in well-dispersed dopant-free ZnO nanoparticles and density functional theory calculation, *J. Alloy. Compd.* 739 (2018) 1080–1088.
- [50] M.T. Efa, T. Imae, Hybridization of carbon-dots with ZnO nanoparticles of different sizes, *J. Taiwan Inst. Chem. Eng.* 92 (2018) 112–117.
- [51] Q. Tian, W. Wu, S. Yang, J. Liu, W. Yao, F. Ren, C. Jiang, Zinc Oxide Coating Effect for the Dye Removal and Photocatalytic Mechanisms of Flower-Like MoS₂ Nanoparticles, *Nanoscale Res. Lett.* 12 (2017) 221–230.

- [52] Y. Liu, Q. Zhang, M. Xu, H. Yuan, Y. Chen, J. Zhang, K. Luo, J. Zhang, B. You, Novel and efficient synthesis of Ag-ZnO nanoparticles for the sunlight-induced photocatalytic degradation, *Appl. Surf. Sci.* 476 (2019) 632–640.
- [53] A. El Golli, M. Fendrich, N. Bazzanella, C. Dridi, A. Miotello, M. Orlandi, Wastewater remediation with ZnO photocatalysts: Green synthesis and solar concentration as an economically and environmentally viable route to application, *J. Environ. Manag.* 286 (2021) 112226–112237.
- [54] C.K. Zagal-Padilla, S.A. Gamboa, Optoelectronic characterization of ZnO obtained by green synthesis of Zn-salt precursor in parsley extract, *J. Alloy. Compd.* 767 (2018) 932–937.
- [55] V. Koutu, L. Shastri, M.M. Malik, Effect of NaOH concentration on optical properties of zinc oxide nanoparticles, *Mater. Sci. -Pol.* 34 (2016) 819–827.
- [56] E.D.M. Isa, K. Shameli, N.W.C. Jusoh, R. Hazan, Rapid photodecolorization of methyl orange and rhodamine B using zinc oxide nanoparticles mediated by pullulan at different calcination conditions, *J. Nanostruct. Chem.* 11 (2021) 187–202.
- [57] H. Gao, C. Zheng, H. Yang, X. Niu, S. Wang, Construction of a CQDs/Ag₃PO₄/BiPO₄ Heterostructure Photocatalyst with Enhanced Photocatalytic Degradation of Rhodamine B under Simulated Solar Irradiation, *Micromachines* 10 (2019) 557–573.
- [58] M. Ahmad, W. Rehman, M.M. Khan, M.T. Qureshi, A. Gul, S. Haq, R. Ullah, A. Rab, F. Menaa, Phytogetic fabrication of ZnO and gold decorated ZnO nanoparticles for photocatalytic degradation of Rhodamine B, *J. Environ. Chem. Eng.* 9 (2021) 104725–104733.
- [59] T. Chankhanittha, S. Nanan, Visible-light-driven photocatalytic degradation of ofloxacin (OFL) antibiotic and Rhodamine B (RhB) dye by solvothermally grown ZnO/Bi₂MoO₆ heterojunction, *J. Colloid Interface Sci.* 582 (2021) 412–427.
- [60] C. Yi, Z. Yu, Q. Ren, X. Liu, Y. Wang, X. Sun, S. Yin, J. Pan, X. Huang, Nanoscale ZnO-based photosensitizers for photodynamic therapy, *Photo Photodyn. Ther.* 30 (2020) 101694–101700.
- [61] K.A. Adegoke, M. Iqbal, H. Louis, O.S. Bello, Synthesis, characterization and application of CdS/ZnO nanorod heterostructure for the photodegradation of Rhodamine B dye, *Mater. Sci. Energy Technol.* 2 (2019) 329–336.
- [62] N. Siva, D. Sakthi, S. Ragupathy, V. Arun, N. Kannadasan, Synthesis, structural, optical and photocatalytic behavior of Sn doped ZnO nanoparticles, *Mater. Sci. Eng. B* 253 (2020) 114497–114505.
- [63] A. Eka Putri, L. Roza, S. Budi, A. Ali Umar, V. Fauzia, Tuning the photocatalytic activity of nanocomposite ZnO nanorods by shape-controlling the bimetallic AuAg nanoparticles, *Appl. Surf. Sci.* 536 (2021) 147847–147858.
- [64] P. Xu, P. Wang, Q. Wang, R. Wei, Y. Li, Y. Xin, T. Zheng, L. Hu, X. Wang, G. Zhang, Facile synthesis of Ag₂O/ZnO/rGO heterojunction with enhanced photocatalytic activity under simulated solar light: Kinetics and mechanism, *J. Hazard. Mater.* 403 (2021) 124011–124023.
- [65] R. Shyamala, L. Gomathi Devi, Reduced graphene oxide/SnO₂ nanocomposites for the photocatalytic degradation of rhodamine B: Preparation, characterization, photosensitization, vectorial charge transfer mechanism and identification of reaction intermediates, *Chem. Phys. Lett.* 748 (2020) 137385–137396.
- [66] L. Zhang, Y. Meng, H. Shen, J. Li, C. Yang, B. Xie, S. Xia, Photocatalytic degradation of rhodamine B by Bi₂O₃@LDHs S-scheme heterojunction: Performance, kinetics and mechanism, *Appl. Surf. Sci.* 567 (2021) 150760–150772.
- [67] A.A. Isari, A. Payan, M. Fattahi, S. Jorfi, B. Kakavandi, Photocatalytic degradation of rhodamine B and real textile wastewater using Fe-doped TiO₂ anchored on reduced graphene oxide (Fe-TiO₂/rGO): Characterization and feasibility, mechanism and pathway studies, *Appl. Surf. Sci.* 462 (2018) 549–564.